

## Article

# Novel C-2 Symmetric Molecules as $\alpha$ -Glucosidase and $\alpha$ -Amylase Inhibitors: Design, Synthesis, Kinetic Evaluation, Molecular Docking and Pharmacokinetics

Danish Shahzad <sup>1</sup>, Aamer Saeed <sup>1,\*</sup>, Fayaz Ali Larik <sup>1</sup>, Pervaiz Ali Channar <sup>1</sup>, Qamar Abbas <sup>2</sup>, Mohamed F. Alajmi <sup>3</sup>, M. Ifzan Arshad <sup>1</sup>, Mauricio F. Erben <sup>4</sup>, Mubashir Hassan <sup>5</sup>, Hussain Raza <sup>5</sup>, Sung-Yum Seo <sup>5</sup> and Hesham R. El-Seedi <sup>6</sup>

<sup>1</sup> Department of Chemistry, Quaid-I-Azam University, Islamabad 45320, Pakistan; danish.scientist.shahzad@gmail.com (D.S.); fayazali@chem.qau.edu.pk (F.A.L.); mrpervaiz@gmail.com (P.A.C.); ifzan\_ifzan@yahoo.com (M.I.A.)

<sup>2</sup> Department of Physiology, University of Sindh, Jamshoro 76080, Pakistan; qamar.abbas.qau@gmail.com

<sup>3</sup> Department of Pharmacognosy, College of Pharmacy, King Saud University, Riyadh 11451, Saudi Arabia; malajmii@ksu.edu.sa

<sup>4</sup> CEQUINOR (UNLP, CONICET-CCT La Plata), Departamento de Química, Facultad de Ciencias Exactas, Universidad Nacional de La Plata, Boulevard 120 e/60 y 64 N°1465, La Plata 1900, Argentina; erbenmf@gmail.com

<sup>5</sup> Department of Biological Sciences, College of Natural Sciences, Kongju National University, 56 Gongjudehak-Ro, Gongju, Chungnam 32588, Korea; mubashirhassan\_gcul@yahoo.com (M.H.); hussain\_solangi@yahoo.com (H.R.); dnalove@kongju.ac.kr (S.-Y.S.)

<sup>6</sup> Pharmacognosy Group, Department of Medicinal Chemistry, Biomedical Center (BMC), Uppsala University, SE-751 23 Uppsala, Sweden; Hesham.El-Seedi@fkog.uu.se

\* Correspondence: aamersaeed@yahoo.com; Tel.: +92-51-9064-2128; Fax: +92-51-9064-2241

Received: 8 March 2019; Accepted: 2 April 2019; Published: 17 April 2019



**Abstract:** A series of symmetrical salicylaldehyde-bishydrazine azo molecules, **5a–5h**, have been synthesized, characterized by <sup>1</sup>H-NMR and <sup>13</sup>C-NMR, and evaluated for their in vitro  $\alpha$ -glucosidase and  $\alpha$ -amylase inhibitory activities. All the synthesized compounds efficiently inhibited both enzymes. Compound **5g** was the most potent derivative in the series, and powerfully inhibited both  $\alpha$ -glucosidase and  $\alpha$ -amylase. The IC<sub>50</sub> of **5g** against  $\alpha$ -glucosidase was  $0.35917 \pm 0.0189 \mu\text{M}$  (standard acarbose IC<sub>50</sub> =  $6.109 \pm 0.329 \mu\text{M}$ ), and the IC<sub>50</sub> value of **5g** against  $\alpha$ -amylase was  $0.4379 \pm 0.0423 \mu\text{M}$  (standard acarbose IC<sub>50</sub> =  $33.178 \pm 2.392 \mu\text{M}$ ). The Lineweaver-Burk plot indicated that compound **5g** is a competitive inhibitor of  $\alpha$ -glucosidase. The binding interactions of the most active analogues were confirmed through molecular docking studies. Docking studies showed that **5g** interacts with the residues Trp690, Asp548, Arg425, and Glu426, which form hydrogen bonds to **5g** with distances of 2.05, 2.20, 2.10 and 2.18 Å, respectively. All compounds showed high mutagenic and tumorigenic behaviors, and only **5e** showed irritant properties. In addition, all the derivatives showed good antioxidant activities. The pharmacokinetic evaluation also revealed promising results

**Keywords:** bis-azo Schiff bases; dual inhibitor;  $\alpha$ -glucosidase inhibitor;  $\alpha$ -amylase; antioxidant; SAR; chemo-informatics; kinetic mechanism; molecular docking

## 1. Introduction

Diabetes mellitus (DM) is a metabolic disorder that poses a serious threat to human health across the globe [1]. In particular, type 2 diabetes mellitus (T2DM) is widely encountered in aged people [2]. An imbalance in the transport of glucose is the main factor leading to diabetes [3]. An abrupt increase

in the glucose level is the major cause of T2DM. Changes in social norms and a lack of proper education regarding a balanced diet are among the main causes of DM [4]. According to the World Health Organization, at least 2.8% of the world's population suffered from T2DM in 2000, and it is estimated that by 2030, this percentage will almost double [5]. The drugs approved by the U.S. FDA for the treatment of diabetes can be categorized into five classes: Biguanides, thiazolidinediones, sulfonylureas, meglitinides and  $\alpha$ -glucosidase inhibitors (AGIs) [6]. The efficacy and sustainability of some drugs are not sufficient. Therefore, the identification of more effective and safer anti-diabetic drugs is of great importance. Several AGIs, such as acarbose (Glucobay<sup>®</sup>), voglibose (Volix<sup>®</sup>, Basen<sup>®</sup>) and miglitol (Glyset<sup>®</sup>) (Figure 1), can reversibly inhibit  $\alpha$ -glucosidase, consequently delaying the absorption of sugars from the gut, and they have been used clinically for the treatment of DM [7].

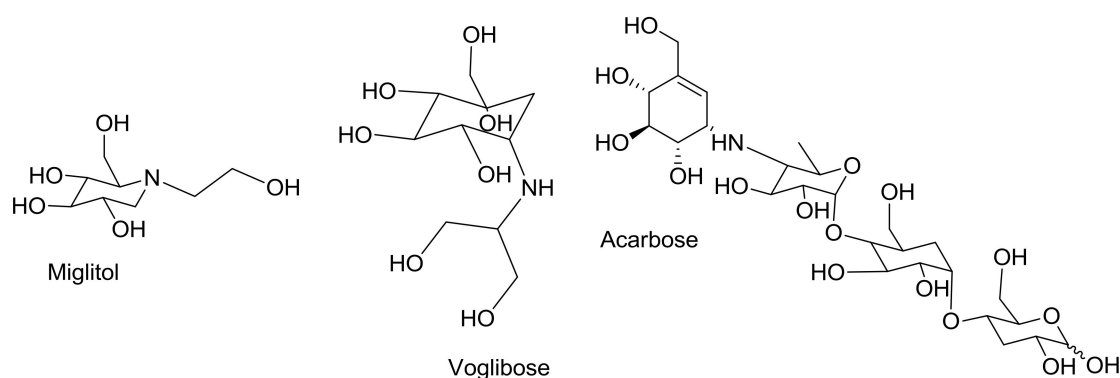


**Figure 1.** Structures of some of the available  $\alpha$ -glucosidase inhibitors.

There commercially available AGIs are associated with certain drawbacks, such as requiring tedious, multistep syntheses; for example voglibose is prepared via a 13-step procedure from (–) shikimic acid, and miglitol is prepared in 13 steps from (R)-methyl 2-benzamido-3-((*tert*-butyldimethylsilyl)oxy)propanoate. Moreover, these AGIs also show some serious adverse effects, including causing flatulence and diarrhoea [8].

To control postprandial glucose levels in T2DM patients, AGIs must be administered. AGIs assist in controlling the progress of hyperglycaemia and hyperinsulinaemia by diverting the workload from pancreatic cells. Postprandial hyperglycaemia (PPHG), if not cured properly and in a timely manner, can lead to life-threatening complications, such as cardiovascular disease and hypertension-related disorders [9]. Acarbose was the first AGI and was made commercially available in 1990. Japanese regulatory agencies approved voglibose as a new AGI in 1994, and two years later, American regulatory agencies approved miglitol as a potent anti-diabetic agent [10]. Among these three AGIs (acarbose, voglibose and miglitol), acarbose has promising effects on several intestinal enzymes; for example, it mainly inhibits  $\alpha$ -amylases, including glucoamylase (90%), sucrose (65%), maltase (60%) and isomaltase (10%) [11].  $\alpha$ -Glucosidase is a membrane-bound enzyme found in intestinal cells that catalyses the production of glucose from a carbohydrate source [12] and  $\alpha$ -Glucosidase cleaves  $\alpha$ -glycosidic bonds. Glucosidase inhibitors can be used as first-line drugs for the treatment of T2DM, because they can lower the rate of carbohydrate absorption and suppress postprandial hyperglycaemia [13–17].

Schiff bases, also known as imines or azomethines, are considered a privileged class of organic compounds and have extensive applications in the fields of biology [18,19], catalysis [20], materials chemistry [21] and inorganic [22] and analytical chemistry [23]. These compounds possess a wide range of biological activities, such as antibacterial, antifungal, antimalarial, anticancer, antitubercular, anti-inflammatory, and antiviral activities [24]. Schiff bases are key precursors in the synthesis of a wide variety of metal complexes, and Schiff base-metal complexes are stable in nature and are useful in non-linear optics (NLOs). Salicylaldehyde-derived Schiff bases have attracted substantial attention, because they exhibit promising effects against microbes [25].

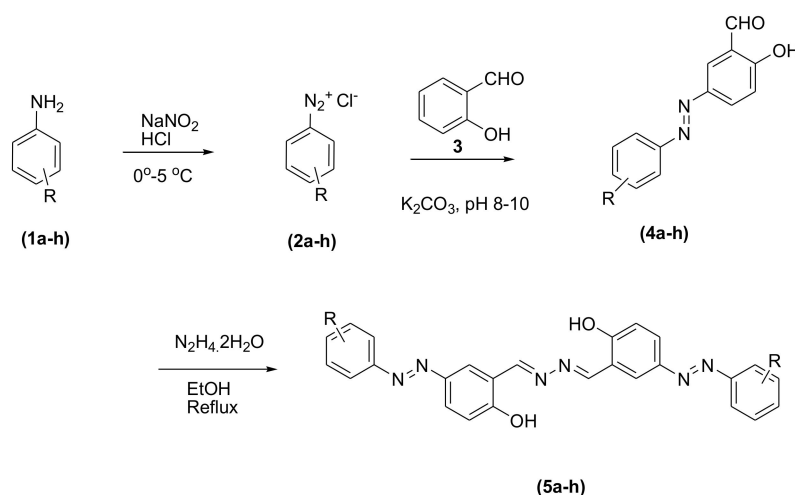
Azo dyes are key chromophores in the chemical industry as dyes and pigments [26], food additives [27], indicators [28], radical initiators [29] and therapeutic agents [30]. Azo azomethine compounds are commonly prepared by the condensation of a primary amine or hydrazine with an aromatic aldehyde or ketone-linked  $-N=N-$  chromophore [31]. Azo ligands are considered robust and chemically stable compounds, and they have been thoroughly investigated in the dye and photoelectrochemical fields [32]. Besides a number of negative features attached to azo compounds, such as toxicity and non-biodegradability, there are several favorable aspects that make them medically attractive compounds. These include the specific azoreduction in vivo, site specific drug delivery of polymeric azo compound in the colon diseases, such as colitis and irritable bowel syndrome Reductive degradation and subsequent splitting of the azo bond Occur in the colon, and therefore they are highly site-specific. Similarly, the azo pro-drugs are reduced to the corresponding amines that are exact therapeutics, for example, 5-aminosalicylic acid derivatives that exhibit anti-inflammatory and cytoprotective potency [33]. FP-21399 is another azo molecule which exhibits anti-HIV potency by inhibiting HIV envelope glycoprotein-mediated membrane fusion that precedes virus infiltration into the cell [34]. There are a limited number of studies on the anti-diabetic and pharmacodynamic properties of salicylaldehyde-derived bis-azo Schiff base ligands.

Herein, we develop a synthetic route to construct new bis-azo ligands using salicylaldehyde as a key precursor. The final products contain a bis-azo group, four aromatic rings, two rings bearing hydroxyl groups and two rings bearing electron-withdrawing substituents.

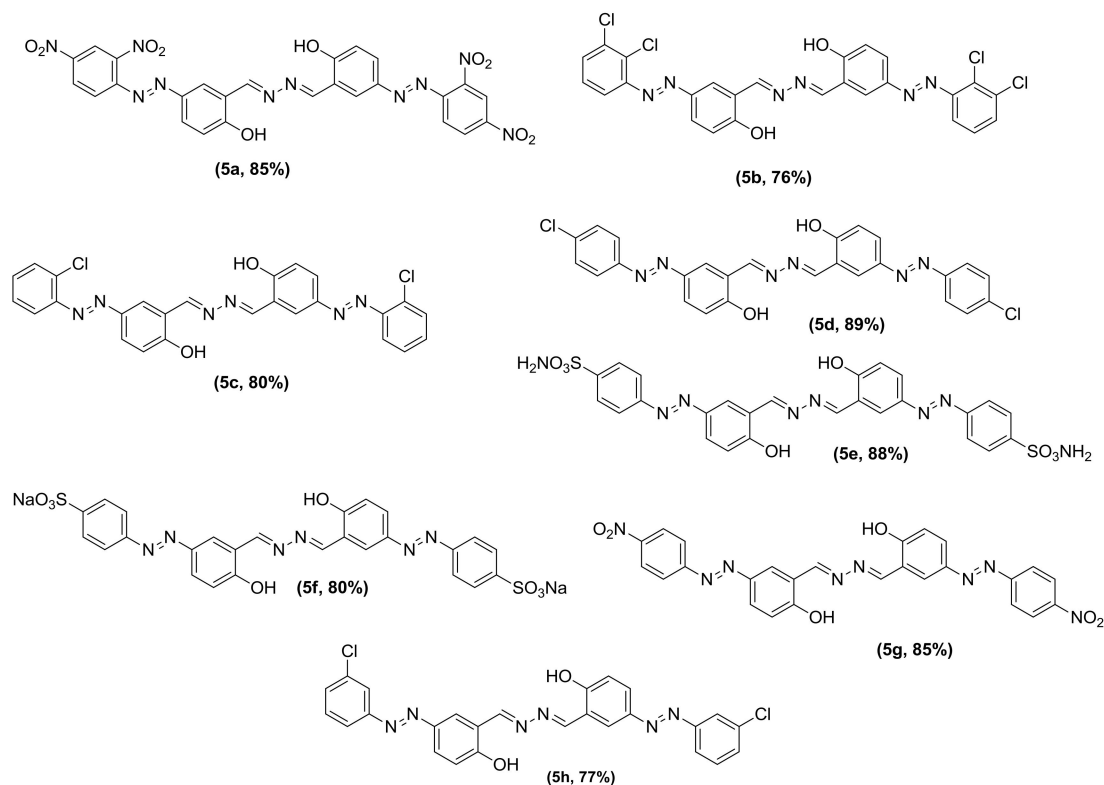
These ligands were selected for two reasons: (i) To provide new acyclic salicylaldehyde-based bis-azo-containing Schiff base ligands, and (ii) to investigate their inhibitory activities against  $\alpha$ -amylase and  $\alpha$ -glucosidase to uncover their antioxidant potential, the kinetics of their enzyme inhibition, their pharmacodynamics (chemo-informatics and Lipinski's rule validation), their initial structure-activity relationships and their binding affinities by exploiting molecular docking.

## 2. Results and Discussion

The synthesis of the bis-azo dyes containing azomethine is depicted in Scheme 1, and the structures and yields of the compounds are shown in Scheme 2. Appropriately substituted anilines (**1a–h**) were used as the starting materials, and the amine group was converted into the diazonium salt using  $\text{NaNO}_2$  and drops of  $\text{HCl}$ . The diazonium salts (**2a–h**) were then coupled with salicylaldehyde under mildly basic conditions to afford **4a–h**. The aldehyde groups of **4a–h** were converted to the corresponding imine with hydrazine hydrate using ethanol to afford the desired products (**5a–h**) in encouraging yields.



**Scheme 1.** The synthetic route towards novel symmetrical compounds (**5a–h**).



**Scheme 2.** Structures and yields of synthesized symmetrical molecules (5a–h).

The synthesized compounds were characterized through  $^1\text{H}$ -NMR and  $^{13}\text{C}$ -NMR spectroscopy. The signal at approximately 9.56 ppm was attributed to the azomethine proton. The phenolic proton appeared at 5–6 ppm. The signals appearing at 7–8 ppm were attributed to protons on the phenyl ring. The signals in the  $^{13}\text{C}$ -NMR spectra from 160–170 ppm were assigned to the carbon of the imine moiety. The carbons bearing electron-withdrawing groups appeared downfield, and the  $\text{sp}^2$  carbons of the phenyl rings appeared from approximately 140–120 ppm.

Azomethine-linked salicylaldehyde is widely recognized as a bioactive moiety. These newly synthesized, bis-azo salicylaldehyde-based Schiff bases inhibit  $\alpha$ -glucosidase and  $\alpha$ -amylase to various degrees. To elucidate the electronic influence on enzyme inhibition, substrates representing almost all possible substitution patterns of the azo group on the phenyl ring were explored. The search for new, potent and safe anti-diabetic agents will remain an important and challenging task for medicinal chemists. Synthesized derivatives 5a–h are structurally similar to each other, and they only differ in the position of the electron-withdrawing group on the phenyl ring. However, these ligands all share a common feature: The presence of two hydroxyl groups, which are pivotal to the inhibition of  $\alpha$ -glucosidase and  $\alpha$ -amylase. The azomethine moiety is considered one of the most intriguing structural entities in medicinal chemistry, because it can interact with the target protein of the enzyme via non-covalent interactions by serving as a hydrogen bond acceptor. Interestingly, compound 5g, which is a non-halogenated derivative in this series, exhibited the highest inhibitory potential against both enzymes ( $\alpha$ -glucosidase and  $\alpha$ -amylase), and it was a dual inhibitor of these two diabetes-promoting enzymes [35]. The  $\text{IC}_{50}$  values of 5g were found to be several folds better than those of acarbose, which was used as a standard (Table 1).

**Table 1.**  $\alpha$ -Glucosidase and  $\alpha$ -amylase inhibitory activities of compounds **5a–h**.

Inhibitor	$\alpha$ -Glucosidase ( $\mu$ M)	$\alpha$ -Amylase ( $\mu$ M)
<b>5a</b>	$0.547 \pm 0.0289$	$8.541 \pm 0.653$
<b>5b</b>	$5.345 \pm 0.2826$	$28.373 \pm 2.171$
<b>5c</b>	$8.061 \pm 0.4263$	$9.5482 \pm 0.730$
<b>5d</b>	$19.521 \pm 1.0321$	$9.7183 \pm 0.863$
<b>5e</b>	$0.367 \pm 0.01941$	$28.4828 \pm 2.081$
<b>5f</b>	$1.841 \pm 0.09738$	$4.2861 \pm 0.328$
<b>5g</b>	$0.359 \pm 0.0189$	$0.4379 \pm 0.042$
<b>5h</b>	$0.400 \pm 0.0211$	$0.5902 \pm 0.012$
<b>Acarbose</b>	$6.109 \pm 0.329$	$33.178 \pm 2.392$

Values are expressed as the mean  $\pm$  SEM; SEM = Standard Error of the Mean.

Nitro-substitution is found in a number of marketed drugs such as Azomycin, Nifurtimox, Benznidazole, Tinidazole, Fexinidazole, Ventetoclax, Delamanid, Entacapone etc. Similarly, there are several therapeutic agents containing a nitro group with bioreductive potentials, such as Paclitaxel prodrug, Tarloxotinib, BTZ043, Evofosfamide, CB-1954 and KS119 [36]. Nevertheless, the nitro group is considered as both a pharmacophore and a toxicophore (hepatotoxic, mutagenic). Compound **5g** possessed a nitro group at the para position of the phenyl ring and showed the most potent inhibition. Compound **5d**, which possessed a chloride at the para position of the phenyl ring, showed the weakest inhibition in the case of  $\alpha$ -glucosidase, indicating that the nature of the electronic group substantially influenced the inhibitory effect. A nitro group can induce great charge density by pulling electrons from the aromatic ring via a resonance effect, while the substituent on compound **5d** can also shift the electron cloud via an inductive effect, but the charge separation will be greater in the case of **5g**. In the case of  $\alpha$ -amylase inhibition, compound **5e** displayed the weakest inhibition, which can be attributed to the presence of a sulfonamide group at the para position of the phenyl ring. All the compounds showed significant inhibition and can serve as lead molecules in the design of DM inhibitors.

### 2.1. Kinetic Analysis

To understand the inhibition mechanism of the synthesized compounds on  $\alpha$ -glucosidase, an inhibition kinetics study was performed. The inhibition type and an inhibition constant of the most potent compound, **5g**, based on our  $IC_{50}$  results, were determined. In our evaluation of the kinetics of the enzyme, the Lineweaver-Burk plot of  $1/V$  versus  $1/[S]$  in the presence of different inhibitor concentrations gave a series of straight lines. The Lineweaver-Burk plot of compound **5g** showed that  $V_{max}$  remains the same without significantly affecting the slopes.  $K_m$  increases with increasing concentration, while  $V_{max}$  remains essentially constant. This behavior indicates that **5g** inhibits the  $\alpha$ -glucosidase in a competitive manner (Figure 2A). Second, as shown in Figure 2B, the plot of the slope against the concentration of **5g** provided the EI dissociation constant.  $K_i$  was calculated from the concentration of **5g** versus the slope, and  $K_i$  was found to be  $3.865 \mu$ M.

### 2.2. Free Radical Scavenging

The DPPH free radical scavenging ability of each of the synthesized compounds was evaluated. Compounds **5d**, **5f** and **5g** did not show significant scavenging potencies (%); however, the other compounds showed significant radical scavenging potentials at a concentration of  $100 \mu$ g/mL (Figure 3).

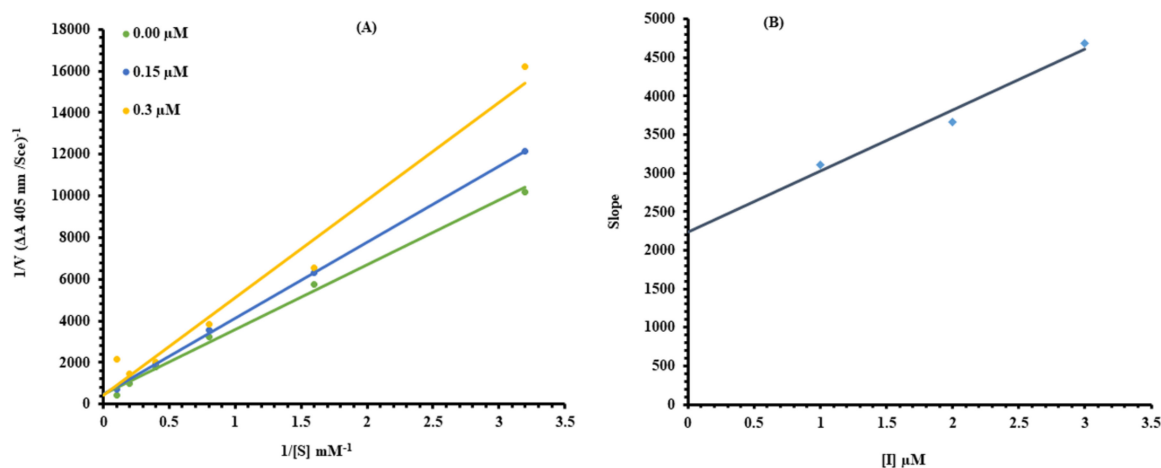


**Figure 2.** Lineweaver-Burk plots for the inhibition of  $\alpha$ -glucosidase by compound 5g (A) The tested concentrations of 5g were 0.00, 0.15, and 0.3  $\mu\text{M}$ ; the concentrations of the substrate (p-nitrophenyl- $\alpha$ -D glucopyranoside) were 10, 5, 2.5, 1.25, 0.625, and 0.3125 mM. (B) The plots of the slope versus inhibitor concentration are shown as insets and were used to determine the inhibition constants.

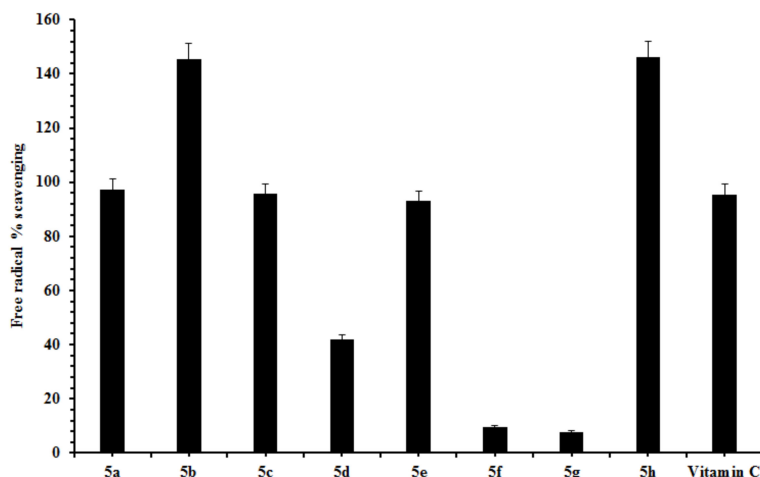


**Figure 3.** Free radical scavenging activity (%) of the synthesized compounds; values are presented as the mean  $\pm$  SEM. All compound concentrations were 100  $\mu\text{g/mL}$ .

### 2.3. Structural Assessment of $\alpha$ -Amylase and $\alpha$ -Glucosidase

$\alpha$ -Amylase (EC#: 3.2.1.1) and  $\alpha$ -glucosidase (EC#: 3.2.1.106) are a class of hydrolyzed proteins that are actively involved as receptor molecules and can be used as targets for therapeutics for the treatment of diabetes. Porcine pancreatic  $\alpha$ -amylase contains 496 residues with 22% helices, 30%  $\beta$  sheets and 47% coil.  $\alpha$ -Glucosidase comprises 811 amino acids with 35% helices, 25%  $\beta$  sheets and 38% coil. X-ray diffraction studies were used to confirm the structures of  $\alpha$ -amylase and  $\alpha$ -glucosidase to resolutions of 1.85  $\text{\AA}$  and 2.04  $\text{\AA}$ , respectively (Figure 4). The Ramachandran plots of  $\alpha$ -amylase and  $\alpha$ -glucosidase indicated that 97.1% and 97.6% of residues, respectively, were present in the well-resolved regions. The Ramachandran graphs showed the high accuracy of the phi ( $\varphi$ ) and psi ( $\psi$ ) angles among the coordinates of target proteins. The Ramachandran graphs of  $\alpha$ -amylase and  $\alpha$ -glucosidase are provided in Supplementary Figure S1A,B, respectively.



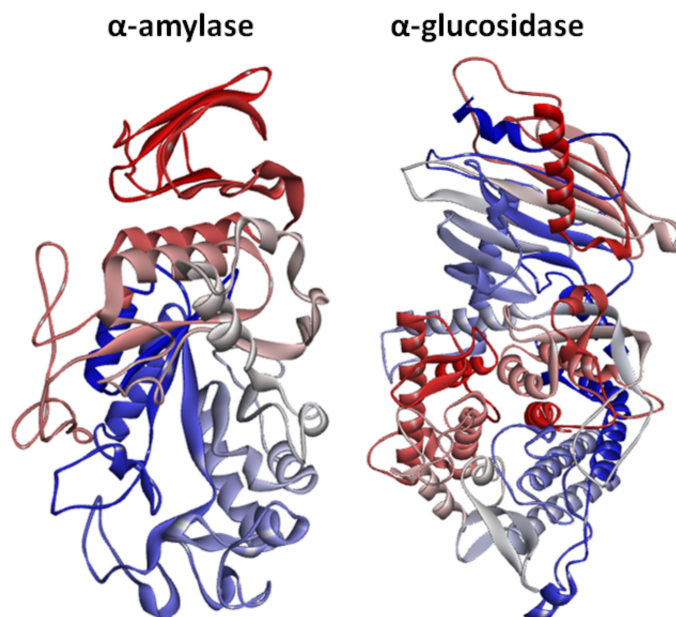


**Figure 4.** The crystal structures of  $\alpha$ -amylase and  $\alpha$ -glucosidase.

#### 2.4. Chemo-Informatics and Lipinski's Rule of Five (RO5) Assessments of the Ligands

The predicted properties, such as the molecular polar surface area (PSA), molar volume, density, polarizability, surface tension, molar refractivity and Lipinski rule violations, were evaluated to determine drug likeness. Prior research has shown that PSA is a significant parameter for predicting drug absorption in drug discovery [37]. The molar refractivity and molecular lipophilicity of drug molecules are important for receptor binding, bioavailability and cellular uptake. Standard values for molar refractivity (40 to 130 cm<sup>3</sup>), molecular weight (160 to 480 g/mol) and PSA (<89 Å<sup>2</sup>) have been reported [38]. The predicted results showed that the molar refractivity and PSA values were comparable to the standard values as mentioned in Table 2. RO5 analysis was used to justify the therapeutic potential of the synthesized compounds. Hydrogen-bonding affinity is an important parameter for evaluating drug permeability [39], and the values of HBA > 10 and HBD > 5 for the ligands result in poor permeation in the body. Our chemo-informatics analyses showed that these ligands possess  $\leq 10$  HBA and  $< 5$  HBD, which suggest good penetration within the body. Moreover, their log*P* values (−2.10) were also comparable to the standard values (< 5). However, there are many examples of RO5 violations among existing drugs [40,41]. The predicted properties are presented in Table 2.

**Table 2.** Cheminformatics Properties.

Properties	5a	5b	5c	5d	5e	5f	5g	5h
Mol. Weight (g/mol)	632.14	584.01	516.09	516.09	638.10	652.04	540.15	516.09
No. HBA	16	8	8	8	16	14	12	8
No. HBD	6	2	2	2	6	2	4	2
Mol. Log <i>P</i>	6.77	11.01	9.82	10.06	4.42	6.26	7.82	10.06
No of SC	0	0	0	0	0	0	0	0
Mol. Vol (Å <sup>3</sup> )	536.68	477.50	446.16	448.00	510.16	515.19	474.01	448.15
Molar Refractivity	154.84	150.61	141.40	141.40	158.32	N/A	143.52	141.40
Density	1.65	1.47	1.36	1.36	1.57	N/A	1.45	1.36
Polarizability	61.38	59.70	56.05	56.05	62.76	N/A	56.89	56.05
Drug Likeness Score	−1.49	−0.51	−0.67	−0.54	−1.22	−1.33	−1.16	−0.73

Abbreviation: Log*P* = Lipophilicity of partition coefficient, SC = stereo centers.

### 2.5. Lead Optimization and Lipophilicity Values

To further evaluate the lead optimization potential of the synthesized compounds. The ligand efficiency (LE), lipophilic ligand efficiency (LLE) and lipophilicity-corrected ligand efficiency (LELP) values of all the synthesized compounds were predicted using the Data Warrior tool. Lipophilicity is a fundamental property for improving the efficacy of lead compounds and identifying drug candidates [42–44]. Hopkins studied the lipophilicities of different compounds and predicted standard values for LE, LLE and LELP on the basis of cLogP values [44]. Suggested acceptable standard values have been reported for LE ( $> \sim 0.30$  kcal/mole/HA), LLE ( $> \sim 0.5$  kcal/mol), and LELP ( $-10 < \text{to} < 10$ ) [44,45]. The predicted LE values of the synthesized compounds were comparable to the standard values. Furthermore, all the compounds showed mutagenic and irritant effects. All the compounds showed potent mutagenic and tumorigenic behavior, whereas only **5e** showed irritant properties. The predicted values for all compounds along with their mutagenic and irritant effects are presented in Table 3.

Table 3. Predicted ligand efficacy values.

Ligands	cLogP	LE	LLE	LELP	Mutagenic	Tumorigenic	Irritant
<b>5a</b>	4.8122	0.24806	3.5055	19.399	high	high	none
<b>5b</b>	10.923	0.28743	−2.960	38.001	high	high	none
<b>5c</b>	9.7106	0.30535	−1.697	31.802	high	high	none
<b>5d</b>	9.7106	0.30535	−1.697	31.802	high	high	none
<b>5e</b>	7.027	0.25421	1.1262	27.642	high	high	high
<b>5f</b>	1.5448	0.28781	7.2633	5.3675	high	high	none
<b>5g</b>	6.6554	0.28044	1.5214	23.732	high	high	none
<b>5h</b>	9.7106	0.30535	−1.697	31.802	high	high	None

### 2.6. Molecular Docking Analysis

The docked ligand-protein complexes were analysed based on their minimum energy values. The compounds showed good binding energy values against  $\alpha$ -amylase and  $\alpha$ -glucosidase (Figure 5). The energy values gave the binding potentials of synthesized compounds against the target proteins. The results showed that **5e** was the most active compound with the best binding energy values for both  $\alpha$ -amylase and  $\alpha$ -glucosidase ( $-10.70$  and  $-11.50$  kcal/mol, respectively) among the tested derivatives. Complexes with **5g** docked showed comparable docking energy values of  $-9.30$  and  $-9.70$  kcal/mol, respectively. The docking energy values of all the docked complexes were calculated using Equation (1), as mentioned in the Supplementary Materials. Prior research has shown that the standard error for Autodock is 2.5 kcal/mol. However, the predicted energy value for each of the docked complexes was less than the standard energy value. Although the synthesized compounds all had the same basic core, most ligands possess good energy values, and no large energy differences were observed. Compound **5g** was the most active in the in vitro analysis; therefore, a structure-activity relationship analysis was performed to evaluate its actual binding within the target proteins.

### 2.7. Structure-Activity Relationship (SAR) Analysis

The active binding region in  $\alpha$ -amylase has been reported previously [46]. The  $\alpha$ -amylase docking results showed that **5g** binds within the active binding region of the target protein and forms three hydrogen bonds. The residues in the active site of  $\alpha$ -amylase that actively participate in hydrogen bonding are Gln63, His201, and Asn301. The benzyl oxygen in **5g** forms a hydrogen bond with Gln63 with a bonding distance of 2.73 Å. Moreover, the hydroxyl and oxygen moieties on the benzene of **5g** form hydrogen bonds with His201 and Asn301 with bond distances of 2.26 and 1.90 Å, respectively. Our docking results were well correlated with a previously published article, confirming the accuracy of our docking results [47]. In  $\alpha$ -glucosidase docking, Trp690, Asp548, Arg425, and Glu426 were the most active residues, as they formed hydrogen bonds to **5g** with distances of 2.05, 2.20, 2.10 and 2.18 Å,



respectively (Figure 6). Based on our docking and kinetic results, it can be hypothesized that **5g** actively binds in the active region of the target protein and has great potential in the treatment of diabetes.

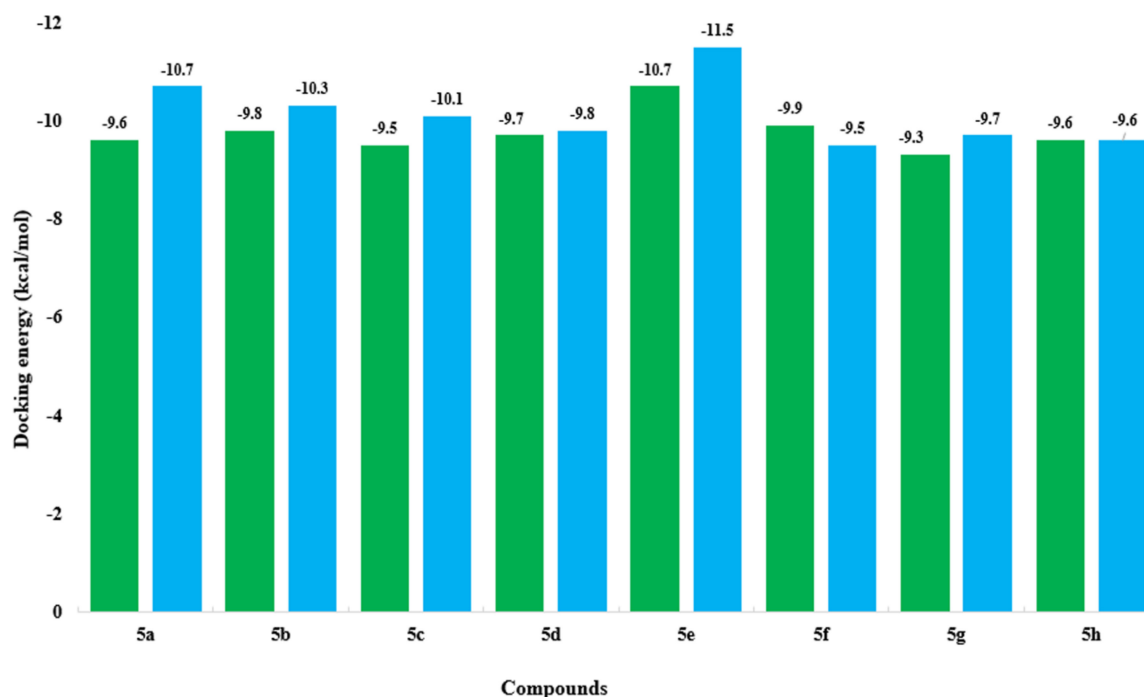


**Figure 5.** Energy graph of both  $\alpha$ -amylase and  $\alpha$ -glucosidase docking (the green bar shows  $\alpha$ -amylase, and the blue bars show  $\alpha$ -glucosidase).

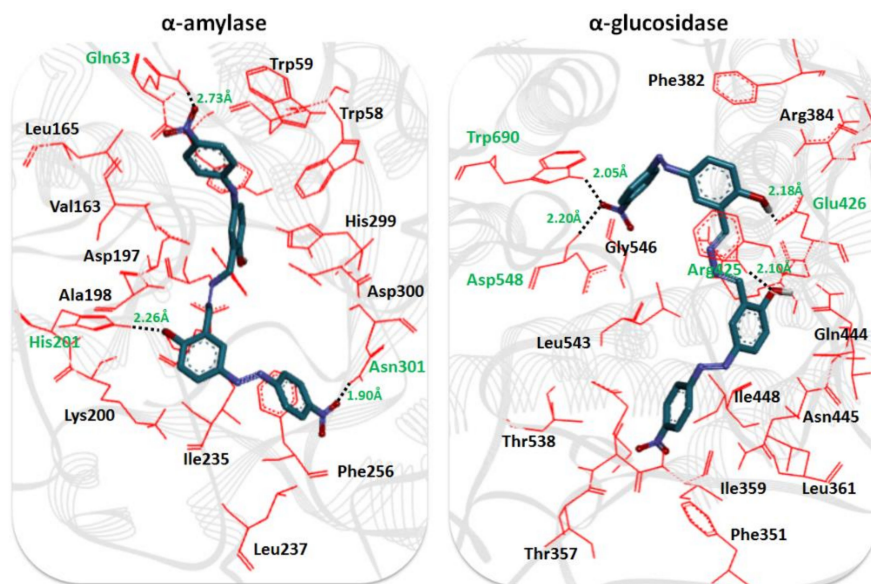


**Figure 6.** Docking of **5g** with  $\alpha$ -amylase and  $\alpha$ -glucosidase.

### 3. Experimental

#### 3.1. Methods and Materials

The  $R_f$  values were determined using aluminium pre-coated silica gel plates (Kiesel 60 F254) from Merck (Darmstadt, Germany). Melting points were measured in open capillaries using a Stuart melting point apparatus (SMP3) and are uncorrected.  $^1\text{H}$ -NMR spectra were determined from DMSO or  $\text{CDCl}_3$  solutions at 300 MHz using a Bruker AM-300 spectrophotometer, and the  $^{13}\text{C}$ -NMR spectra were

determined at 75 MHz using a Bruker 75 MHz NMR from DMSO- $d_6$  or  $CDCl_3$  solutions. Elemental analyses were performed on a LECO CHNS-932 Elemental Analyzer (LECO Corporation, Saint Joseph, MI, USA). All the chemicals used for the syntheses of the compounds were commercially obtained and were used without additional purification.

### 3.2. General Procedure for the Synthesis of Phenolic Azo Dyes (**4a–4j**) and Their Condensation with Hydrazine Dihydrate (**5a–5j**)

Suitably substituted anilines (**1a–1h**) (0.01 mol) were dissolved in 20 mL of water and 3.5 mL of concentrated HCl with stirring at a temperature of 0–5 °C. A solution of  $NaNO_2$  (0.01 mL) in 10 mL of water was promptly added to the aniline solution with continuous and vigorous stirring. The reaction mixture was stirred for 1 h while maintaining the temperature in the same range. After 1 h, the reaction mixture was checked for the completeness with a paper chromatogram using water as the mobile phase. The dried chromatogram was sprayed with a solution of *p*-*N,N*-dimethyl aminobenzaldehyde in ethanol. Upon completion of the reaction, the diazonium salts (**2a–2h**) were stored in a freezer.

Salicylaldehyde **3** (0.01 mL) was dissolved in water (15 mL) with  $K_2CO_3$  (1.5 g) and kept in an ice bath at 0–5 °C with stirring. The diazo solution was added dropwise to the stirred solution of salicylaldehyde over 45 min, and the pH was maintained above 8. The progress of the reaction was monitored by paper chromatography using H-acid solution in alkaline media. Upon completion, the solids were isolated by filtration and dried in an oven at 70 °C for 3 h to afford the 4-(benzeneazo)salicylaldehyde derivatives (**3a–3h**) in 85–92% yields. When mixtures of regioisomers were obtained, they were separated by column chromatography. Then, 0.01 mol (0.5 g) of hydrazine dihydrate ( $N_2H_4 \cdot 2H_2O$ ) was slowly added to a solution of 0.02 mol of the appropriate 4-(benzeneazo)salicylaldehyde derivative (**5a–5h**). After refluxing the reaction mixture for 3 h, the mixture was cooled, and the precipitate was collected by filtration. The precipitate was washed several times with ethanol, crystallized from ethanol, and dried at 50 °C overnight (yields > 70%).

#### (*E*)-2,2'-((1*E*,1'*E*)-Hydrazine-1,2-diylidenebis(methanylylidene))bis(4-((*E*)-(2,4-dinitrophenyl)diazenyl)phenol) (**5a**)

Light yellow crystalline solid, mp = 275 °C, Yield 95%,  $R_f$  = 0.45 (*n*-Hexane: Ethyl acetate 6:4),  $^1H$ -NMR (DMSO- $d_6$ , 300 MHz);  $\delta$  (ppm) 11.81 (s, 2H, Ar-OH), 9.17 (s, 2H, =N-H), 8.69 (d, 2H, Ar-H,  $J$  = 1.9 Hz), 8.48 (d, 2H, Ar-H,  $J$  = 1.99 Hz), 8.01 (dd, 2H, Ar-H,  $J$  = 8.7 Hz,  $J$  = 2.1 Hz), 7.94 (dd, 2H, Ar-H,  $J$  = 8.6 Hz,  $J$  = 1.7 Hz), 7.87 (d, 2H, Ar-H, 8.9 Hz), 7.21 (d, 2H, Ar-H,  $J$  = 9 Hz),  $^{13}C$ -NMR (75 MHz DMSO- $d_6$ )  $\delta$  (ppm), 161.94 (C=O), 161.83, 152.17, 150.62, 145.58, 144.87, 127.68, 127.21, 125.48, 122.35, 119.57, 118.27, 118.11, Anal. Calcd. for  $C_{26}H_{16}N_{10}O_{10}$ : C, 49.69; H, 2.57; N, 22.29; found: C, 49.60; H 2.60; N, 22.25.

#### (*E*)-2,2'-((1*E*,1'*E*)-Hydrazine-1,2-diylidenebis(methanylylidene))bis(4-((*E*)-(2,3-dichlorophenyl)diazenyl)phenol) (**5b**)

Dark yellow crystalline solid, mp = 222 °C, Yield 89%,  $R_f$  = 0.62 (*n*-Hexane: Ethyl acetate 6:4),  $^1H$ -NMR ( $CDCl_3$ , 300 MHz);  $\delta$  (ppm) 11.82 (s, 2H, Ar-OH), 9.15 (s, 2H, =N-H), 8.40 (d, 2H, Ar-H,  $J$  = 2.0 Hz), 7.96 (dd, 2H, Ar-H,  $J$  = 8.7 Hz,  $J$  = 2.1 Hz), 7.89–7.59 (m, 6H, Ar-H), 7.21 (d, 2H, Ar-H,  $J$  = 8.92 Hz),  $^{13}C$ -NMR (75 MHz  $CDCl_3$ )  $\delta$  (ppm), 161.96 (C=O), 161.84, 154.19, 150.61, 130.11, 133.21, 128.64, 127.21, 125.48, 122.36, 119.53, 118.11, 116.21 Anal. Calcd. for  $C_{26}H_{16}Cl_4N_6O_2$ : C, 53.27; H, 2.75; N, 14.34; found: C, 53.20; H, 2.83; N, 14.40.

#### (*E*)-2,2'-((1*E*,1'*E*)-Hydrazine-1,2-diylidenebis(methanylylidene))bis(4-((*E*)-(2-chlorophenyl)diazenyl)phenol) (**5c**)

Dark reddish-orange crystalline solid, mp = 195 °C, Yield 85%,  $R_f$  = 0.75 (*n*-Hexane: Ethyl acetate 6:4),  $^1H$ -NMR ( $CDCl_3$ , 300 MHz);  $\delta$  (ppm) 11.81 (s, 2H, Ar-OH), 9.14 (s, 2H, =N-H), 8.38 (d, 2H, Ar-H,  $J$  = 2.0 Hz), 7.92 (dd, 2H, Ar-H,  $J$  = 8.60 Hz,  $J$  = 2.0 Hz), 7.89–7.49 (m, 8H, Ar-H), 7.20 (d, 2H, Ar-H,  $J$  = 8.98 Hz),  $^{13}C$ -NMR (75 MHz  $CDCl_3$ )  $\delta$  (ppm) 161.90 (C=O), 161.82, 152.12, 150.51, 127.66, 127.21,

125.47, 132.22, 124.22, 129.26, 128.38, 119.58, 118.11. Anal. Calcd. for  $C_{26}H_{18}Cl_2N_6O_2$ : C, 60.36; H, 3.51; N, 16.24; found: C, 60.42; H, 3.59; N, 16.31.

(*E*)-2,2'-((1*E*,1'*E*)-Hydrazine-1,2-diylidenebis(methanylylidene))bis(4-((*E*)-(4-chlorophenyl)diazenyl)phenol) (**5d**)

Light yellow crystalline solid, mp = 205 °C, Yield 86%,  $R_f$  = 0.70 (*n*-Hexane: Ethyl acetate 6:4);  $^1H$ -NMR ( $CDCl_3$ , 300 MHz);  $\delta$  (ppm) 11.81 (s, 2H, Ar-OH), 9.14 (s, 2H, =N-H), 8.37 (d, 2H, Ar-H,  $J$  = 2.1 Hz), 7.92 (dd, 2H, Ar-H,  $J$  = 8.61 Hz,  $J$  = 2.1 Hz), 7.79 (dd, 8H, Ar-H,  $J$  = 8.51 Hz), 7.19 (d, 2H, Ar-H,  $J$  = 8.98 Hz),  $^{13}C$ -NMR (75 MHz  $CDCl_3$ )  $\delta$  (ppm) 162.89 (C=O), 161.83, 152.11, 150.59, 136.21, 124.11, 129.21, 127.19, 125.46, 119.57, 118.10, Anal. Calcd. for  $C_{26}H_{18}Cl_2N_6O_2$ : C, 60.36; H, 3.51; N, 16.24; found: C, 60.44; H, 3.60; N, 16.29.

4,4'-((1*E*,1'*E*)-((1*E*,1'*E*)-Hydrazine-1,2-diylidenebis(methanylylidene))bis(4-hydroxy-3,1-phenylene))bis(diazeno-2,1-diyl)dibenzenesulfonamide (**5e**)

Dark orange crystalline solid, mp = 225 °C, Yield 76%,  $R_f$  = 0.70 (Chloroform: Ethanol 9:1);  $^1H$ -NMR ( $DMSO-d_6$ , 300 MHz);  $\delta$  (ppm) 11.83 (s, 2H, Ar-OH), 9.12 (s, 2H, =N-H), 8.38 (d, 2H, Ar-H,  $J$  = 2.0 Hz), 7.99 (dd, 2H, Ar-H,  $J$  = 8.6 Hz,  $J$  = 2.0 Hz), 7.81 (m, 8H, Ar-H), 7.55 (s, 4H), 7.21 (d, 2H, Ar-H,  $J$  = 8.94 Hz),  $^{13}C$ -NMR (75 MHz  $DMSO-d_6$ )  $\delta$  (ppm) 161.93 (C=O), 161.82, 152.16, 150.59, 145.61, 127.65, 127.19, 125.46, 122.35, 119.58, 118.09, Anal. Calcd. for  $C_{26}H_{22}N_8O_6S_2$ : C, 51.48; H, 3.66; N, 18.47; S, 10.57; found: C, 51.42; H, 3.64; N, 18.43; S, 10.52.

Sodium 4,4'-((1*E*,1'*E*)-((1*E*,1'*E*)-hydrazine-1,2-diylidenebis(methanylylidene))bis(4-hydroxy-3,1-phenylene))bis(diazeno-2,1-diyl)dibenzenesulfonate (**5f**)

Bright yellow crystalline solid, m.p = 240 °C, Yield 80 %,  $R_f$  = 0.55 (Chloroform: Ethanol 9:1),  $^1H$ -NMR ( $DMSO-d_6$ , 300 MHz);  $\delta$  (ppm) 11.84 (s, 2H, Ar-OH), 9.16 (s, 2H, =N-H), 8.40 (d, 2H, Ar-H,  $J$  = 2.1 Hz), 7.99 (dd, 2H, Ar-H,  $J$  = 8.7 Hz,  $J$  = 2.1 Hz), 7.82 (m, 8H, Ar-H), 7.23 (d, 2H, Ar-H,  $J$  = 9 Hz),  $^{13}C$ -NMR (75 MHz  $DMSO-d_6$ )  $\delta$  (ppm) 161.96 (C=O), 161.84, 152.17, 150.61, 145.59, 127.67, 127.20, 125.48, 122.36, 119.59, 118.11, Anal. Calcd. for  $C_{26}H_{18}N_6Na_2O_8S_2$ : C, 47.85; H, 2.78; N, 12.88; S, 9.83; Found: C, 47.81; H, 2.72; N, 12.83; S, 9.78.

(*E*)-2,2'-((1*E*,1'*E*)-Hydrazine-1,2-diylidenebis(methanylylidene))bis(4-((*E*)-(4-nitrophenyl)diazenyl)phenol) (**5g**)

Dark brown crystalline solid, m.p = 215 °C, Yield 85%,  $R_f$  = 0.45 (*n*-Hexane: Ethyl acetate 6:4),  $^1H$ -NMR ( $DMSO-d_6$ , 300 MHz);  $\delta$  (ppm) 11.82 (s, 2H, Ar-OH), 9.14 (s, 2H, =N-H), 8.40 (d, 2H, Ar-H,  $J$  = 1.9 Hz), 7.98 (dd, 2H, Ar-H,  $J$  = 8.7 Hz,  $J$  = 2.1 Hz), 7.98 (dd, 8H, Ar-H), 7.21 (d, 2H, Ar-H,  $J$  = 8.9 Hz),  $^{13}C$ -NMR (75 MHz  $DMSO-d_6$ )  $\delta$  (ppm) 161.95 (C=O), 161.82, 152.14, 150.59, 145.57, 127.67, 127.19, 125.46, 122.35, 119.56, 118.09, Anal. Calcd. for  $C_{26}H_{18}N_8O_6$ : C, 57.99; H, 3.37; N, 20.81; found: C, 57.91; H, 3.29; N, 20.89.

(*E*)-2,2'-((1*E*,1'*E*)-Hydrazine-1,2-diylidenebis(methanylylidene))bis(4-((*E*)-(3-chlorophenyl)diazenyl)phenol) (**5h**)

Dark yellow crystalline solid, m.p = 210 °C, Yield 87%,  $R_f$  = 0.65 (*n*-Hexane: Ethyl acetate 6:4),  $^1H$ -NMR ( $CDCl_3$ , 300 MHz);  $\delta$  (ppm) 11.80 (s, 2H, Ar-OH), 9.08 (s, 2H, =N-H), 8.39 (d, 2H, Ar-H,  $J$  = 1.9.0 Hz), 7.98 (dd, 2H, Ar-H,  $J$  = 8.59 Hz,  $J$  = 2.1 Hz), 8.12-7.76 (dd, 8H, Ar-H,  $J$  = 8.61 Hz), 7.21 (d, 2H, Ar-H,  $J$  = 8.90 Hz),  $^{13}C$ -NMR (75 MHz  $CDCl_3$ )  $\delta$  (ppm) 161.96 (C=O), 161.84, 152.18, 150.61, 133.09, 130.89, 130.24, 127.20, 125.48, 123.44, 121.02, 119.59, 118.11, Anal. Calcd. for  $C_{26}H_{18}Cl_2N_6O_2$ : C, 60.36; H, 3.51; N, 16.24; found: C, 60.44; H, 3.59; N, 16.32.

### 3.3. Biological Activity Methods

#### 3.3.1. $\alpha$ -Glucosidase Inhibition Assay

The  $\alpha$ -glucosidase inhibitory activities of the synthesized compounds were evaluated following the method described by Saleem et al., 2014 [33]. Briefly, solutions of the substrate (5 mM, *p*-nitrophenyl- $\alpha$ -D-glucopyranoside, Sigma, St. Louis, MO, USA) and  $\alpha$ -glucosidase (Sigma, St. Louis, MO, USA) were prepared in 100 mM phosphate buffer (pH 7.0) containing 0.2 g/L  $\text{NaN}_3$  and 2 g/L bovine serum albumin. The assay mixtures contained the compound (inhibitors), substrate and enzyme solutions. First, 10  $\mu\text{L}$  of the test compound (dissolved in 1% DMSO) and 50  $\mu\text{L}$  of the enzyme solution were added to a 96-well microplate, and the assay plate was incubated for 5 min at room temperature. Then, 50  $\mu\text{L}$  of the substrate solution was added, and the mixtures were incubated for 10 min at 37 °C. Finally, the reactions were terminated by adding 100  $\mu\text{L}$  of sodium carbonate solution (100 mM). The blank was prepared by adding all the components except the enzyme. The absorbance of was reaction mixture was recorded at 405 nm using a microplate reader (OPTI<sub>Max</sub>, Tunable Micro Plate Reader, Sunnyvale, CA, USA). Acarbose was used as a reference drug. All the reactions were performed in triplicate and repeated three times. Percentage inhibition was calculated using the following equation,

$$\text{Inhibition (\%)} = [(B - S)/B] \times 100 \quad (1)$$

Here, B and S are the absorbances of the blank and sample, respectively. The  $\text{IC}_{50}$  values were calculated by the program Prism 5.0 (GraphPad, San Diego, CA, USA).

#### 3.3.2. $\alpha$ -Amylase Inhibition Assay

The  $\alpha$ -amylase inhibitory activity of sinigrin was determined according to a previously reported method [33] with slight modifications. Briefly, 40  $\mu\text{L}$  of a solution of the test inhibitor and 40  $\mu\text{L}$  of enzyme solution ( $\alpha$ -amylase from porcine pancreas (Sigma A3176-500KU, 089K1661) in a buffer of 0.02 M sodium phosphate at pH 6.9 with 0.006 M sodium chloride) were added to a 1.5-mL Eppendorf tube and incubated for 10 min at room temperature. Then, 40  $\mu\text{L}$  of a starch solution (1% in DMSO) was added to the pre-incubated tubes, and the solutions were incubated for an additional 10 min at 25 °C. Then, 100  $\mu\text{L}$  of DNSA colouring reagent (10 g of sodium potassium tartrate, 1 g of 3,5-dinitrosalicylic acid and 20 mL of 2 N NaOH to a final volume of 100 mL in distilled water) was added, and the mixture was incubated in a boiling water bath for 5 min. After cooling to room temperature, the reaction mixture was diluted to 500  $\mu\text{L}$  using distilled water, and the absorbance was recorded at 540 nm. For non-enzymatic reactions, the assays were performed with a blank containing all of the components except the enzyme. The values of the % inhibition and  $\text{IC}_{50}$  were calculated from the results of the assays using the same procedure as that described for the  $\alpha$ -glucosidase inhibition assays.

#### 3.3.3. Free radical Scavenging Assay

Radical scavenging activity was determined by modifying a previously reported 2,2-diphenyl-1-picrylhydrazyl (DPPH) assay [34,35]. The assay solution consisted of 100  $\mu\text{L}$  of DPPH solution (150  $\mu\text{M}$ ), 20  $\mu\text{L}$  of the test compounds solution at increasing concentrations, and enough DMSO to bring the volume of solution in each well to 200  $\mu\text{L}$ . The reaction mixture was then incubated for 30 min at room temperature. Ascorbic acid (vitamin C) was used as a reference inhibitor. The assay measurements were carried out using a micro plate reader (OPTI<sub>Max</sub>, Tunable) at 520 nm. The reaction rates were compared, and the percentages of inhibition caused by the presence of the test inhibitors were calculated. Each concentration was analysed in three independent experiments run in triplicate.

#### 3.3.4. Kinetic Study of $\alpha$ -Glucosidase

Based on the  $\text{IC}_{50}$  values, the most potent inhibitor, **5g**, was selected for kinetic analysis. A series of experiments was performed to calculate the inhibition kinetics of **5g**. The tested concentrations of

**5g** were 0.00, 0.15 and 0.3. The concentration of substrate, *p*-nitrophenyl- $\alpha$ -D-glucopyranoside, was between 0.3125 and 10 mM in all the kinetics experiments. The pre-incubation and measurement times were the same as those discussed in the  $\alpha$ -glucosidase inhibition assay procedure. The maximal initial velocity was determined from the initial linear portion of absorbance in the first five minutes following the addition of the enzyme at 30 s intervals. The type of inhibition of the enzyme was assessed by preparing Lineweaver-Burk plots of the inverse of the velocities ( $1/V$ ) versus the inverse of the substrate concentration  $1/[S]$  mM<sup>-1</sup>. The EI dissociation constant,  $K_i$ , was determined by the secondary plot of  $1/V$  versus the inhibitor concentration.

### 3.4. Computational Methodology

#### 3.4.1. Selection of Target Proteins from the PDB

The three-dimensional (3D) structures of  $\alpha$ -amylase and  $\alpha$ -glucosidase, with PDBIDs of 1DHK and 4J5T, respectively, were retrieved from the Protein Data Bank (PDB) ([www.rcsb.org](http://www.rcsb.org)). The energies of the target proteins were minimized with an Amber force field by using a conjugate gradient algorithm in UCSF Chimera 1.10.1 (Pettersen et al., 2006). The overall protein architecture and statistical percentages of helices,  $\beta$ -sheets, coils and turns were retrieved from the online server VADAR 1.8 (Willard et al., 2003). The Discovery Studio 4.1 Client (D. Studio, 2008) was used as a visualizing tool to generate graphical depictions of the target proteins.

#### 3.4.2. In-Silico Design of Ligand Structures

The synthesized ligands were sketched using the ACD/ChemSketch tool and minimized using UCSF Chimera 1.10.1. The basic biological properties, such as molecular weight (g/mol), numbers of hydrogen bond acceptors and donors (HBA/D), Log*P*, number of stereo centres, molecular volume (Å<sup>3</sup>), molar refractivity density, polarizability and drug likeness score were evaluated using the online computational tools Molsoft (<http://www.molsoft.com/>) and Molinspiration (<http://www.molinspiration.com/>). Moreover, Lipinski's rule of five was also considered to evaluate the efficacy of the ligand structures. Furthermore, the ligand efficiency (LE), lipophilic ligand efficiency (LLE) and lipophilicity-corrected ligand efficiency (LELP) values of all the ligands were calculated using the Data Warrior tool. Moreover, the mutagenic and irritant risks were assessed using the Data Warrior tool.

#### 3.4.3. Ligand-Based Docking Simulation

Molecular docking experiments were conducted on all the synthesized ligands against  $\alpha$ -amylase and  $\alpha$ -glucosidase using the PyRx docking tool (Dallakyan and Olson, 2015). The grid box-centred parametric values for  $\alpha$ -amylase were adjusted as  $x = -18.44$ ,  $y = -20.91$ ,  $z = 8.22$ , while the size values for all coordinates were adjusted as  $x = 77.93$ ,  $y = 68.98$ , and  $z = 103.65$ , respectively. Similarly, for  $\alpha$ -glucosidase, the grid values were adjusted as center\_x = 102.22, center\_y = 40.10, center\_z = 18.02, while the size values were adjusted as size\_x = 57.60, size\_y = 59.83 and size\_z = 72.29, respectively. A default exhaustiveness value = 8 was used in both docking studies to maximize the binding conformational analysis. The docking poses (100 numbers of runs) for each docking study were adjusted to obtain the best docking results. The selected compound was docked separately and evaluated based on the lowest binding energy (Kcal/mol) and the structure-activity relationship. Graphical depictions of all the docking complexes were prepared using Discovery Studio (2.1.0).

## 4. Conclusions

A series of new bis-azo dyes based on Schiff bases (**5a–5h**) were synthesized and characterized through elemental and spectroscopic techniques. The abilities of the synthesized compounds to inhibit  $\alpha$ -glucosidase and  $\alpha$ -amylase were evaluated. Compounds **5a–5h** all significantly inhibited both of these enzymes. Derivatives **5a–5h** also showed good antioxidant activities. Kinetic studies were

performed to elucidate the modes of inhibition of  $\alpha$ -amylase and  $\alpha$ -glucosidase, and the most potent derivative, **5g**, was a dual inhibitor of these enzymes via competitive inhibition. The binding modes of ligands with the target proteins were explored by molecular docking studies. Pharmacokinetics and chemo-informatics evaluations revealed that the properties of the molecules were similar, and a few of the derivatives in this series can serve as lead molecules in the design of drugs for the treatment of DM.

**Supplementary Materials:** Supplementary Materials are available online.

**Author Contributions:** Conceptualization, A.S.; methodology, P.A.C., D.S.; software, Q.A.; validation, M.H., H.R., M.I.A. and S.-Y.S.; formal analysis, M.F.E.; investigation, P.A.C.; resources, H.R.E.; data curation, Q.A.; writing—original draft preparation, D.S., F.A.L.; writing—review and editing, A.S., H.R.E.; visualization, A.S.; supervision, A.S.; project administration, S.-Y.S.; funding acquisition, H.R.E.-S., M.F.A.

**Funding:** This research was funded by International Scientific Partnership Program (ISPP), grant number ISPP-126. The APC was funded by ISPP.

**Acknowledgments:** The authors wish to express their appreciation to the International Scientific Partnership Program (ISPP) at King Saud University for funding this research work through an ISPP-126 grant awarded to H.R.E.-S. and M.F.A.

**Conflicts of Interest:** The authors declare no conflicts of interest.

## References

1. Wang, G.; Chen, M.; Wang, J.; Peng, Y.; Li, L.; Xie, Z.; Deng, B.; Chen, S.; Li, W. Synthesis, biological evaluation and molecular docking studies of chromone hydrazone derivatives as  $\alpha$ -glucosidase inhibitors. *Bioorg. Med. Chem. Lett.* **2017**, *27*, 2957–2961. [[CrossRef](#)] [[PubMed](#)]
2. Gupta, S.J.; Dutta, S.; Gajbhiye, R.L.; Jaisankar, P.; Sen, A.K. Synthesis, in vitro evaluation and molecular docking studies of novel amide linked triazolyl glycoconjugates as new inhibitors of  $\alpha$ -glucosidase. *Bioorg. Chem.* **2017**, *72*, 11–20. [[CrossRef](#)]
3. Wang, G.; Wang, J.; Xie, Z.; Chen, M.; Li, L.; Peng, Y.; Chen, S.; Li, W.; Deng, B. Discovery of 3, 3-di (indolyl) indolin-2-one as a novel scaffold for  $\alpha$ -glucosidase inhibitors: In silico studies and SAR predictions. *Bioorg. Chem.* **2017**, *72*, 228–233. [[CrossRef](#)] [[PubMed](#)]
4. Chaudhry, F.; Choudhry, S.; Huma, R.; Ashraf, M.; Al-Rashida, M.; Munir, R.; Sohail, R.; Jahan, B.; Munawar, M.A.; Khan, M.A. Hetaryl coumarins: synthesis and biological evaluation as potent  $\alpha$ -glucosidase inhibitors. *Bioorg. Chem.* **2017**, *73*, 1–9. [[CrossRef](#)] [[PubMed](#)]
5. Kasturi, S.; Surarapu, S.; Uppalanchi, S.; Anireddy, J.S.; Dwivedi, S.; Anantaramu, H.S.; Perumal, Y.; Sigalapalli, D.K.; Babu, B.N.; Ethiraj, K.S. Synthesis and  $\alpha$ -glucosidase inhibition activity of dihydroxy pyrrolidines. *Bioorg. Med. Chem. Lett.* **2017**, *27*, 2818–2823. [[CrossRef](#)] [[PubMed](#)]
6. Saeed, A.; Channar, P.A.; Larik, F.A.; Jabeen, F.; Muqadar, U.; Saeed, S.; Flörke, U.; Ismail, H.; Dilshad, E.; Mirza, B. Design, synthesis, molecular docking studies of organotin-drug derivatives as multi-target agents against antibacterial, antifungal,  $\alpha$ -amylase,  $\alpha$ -glucosidase and butyrylcholinesterase. *Inorg. Chim. Acta* **2017**, *464*, 204–213. [[CrossRef](#)]
7. Muraoka, O.; Ying, S.; Yoshikai, K.; Matsuura, Y.; Yamada, E.; Minematsu, T.; Tanabe, G.; Matsuda, H.; Yoshikawa, M. Synthesis of a nitrogen analogue of salacinol and its  $\alpha$ -glucosidase inhibitory activity. *Chem. Pharma Bull.* **2001**, *49*, 1503–1505. [[CrossRef](#)]
8. Arshad, N.; Perveen, F.; Saeed, A.; Channar, P.A.; Farooqi, S.I.; Larik, F.A.; Ismail, H.; Mirza, B. Spectroscopic, molecular docking and structural activity studies of (E)-N'-(substituted benzylidene/methylene) isonicotinohydrazide derivatives for DNA binding and their biological screening. *J. Mol. Struct.* **2017**, *1139*, 371–380. [[CrossRef](#)]
9. Cai, C.Y.; Rao, L.; Rao, Y.; Guo, J.X.; Xiao, Z.Z.; Cao, J.Y.; Huang, Z.S.; Wang, B. Analogues of xanthenes—Chalcones and bis-chalcones as  $\alpha$ -glucosidase inhibitors and anti-diabetes candidates. *Eur. J. Med. Chem.* **2017**, *130*, 51–59. [[CrossRef](#)]
10. Chaudhry, F.; Naureen, S.; Huma, R.; Shaikat, A.; Al-Rashida, M.; Asif, N.; Ashraf, M.; Munawar, M.A.; Khan, M.A. In search of new  $\alpha$ -glucosidase inhibitors: Imidazolylpyrazole derivatives. *Bioorg. Chem.* **2017**, *71*, 102–109. [[CrossRef](#)]



11. Noreen, T.; Taha, M.; Imran, S.; Chigurupati, S.; Rahim, F.; Selvaraj, M.; Ismail, N.H.; Mohammad, J.I.; Ullah, H.; Nawaz, F.; et al. Synthesis of alpha amylase inhibitors based on privileged indole scaffold. *Bioorg. Chem.* **2017**, *72*, 248–255. [[CrossRef](#)] [[PubMed](#)]
12. Balan, K.; Perumal, P.; Sundarabaalaji, N.; Palvannan, T. Synthesis, molecular modeling and biological evaluation of novel 2-allyl amino 4-methyl sulfanyl butyric acid as  $\alpha$ -amylase and  $\alpha$ -glucosidase inhibitor. *J. Mol. Struct.* **2015**, *1081*, 62–68. [[CrossRef](#)]
13. Saeed, A.; Bosch, A.; Bettiol, M.; Nossa González, D.L.; Erben, M.F.; Lamberti, Y. Novel Guanidine Compound against Multidrug-Resistant Cystic Fibrosis-Associated Bacterial Species. *Molecules* **2018**, *23*, 1158. [[CrossRef](#)]
14. Saeed, A.; Shahzad, D.; Larik, F.A.; Channar, P.A.; Mehfooz, H.; Abbas, Q.; Hassan, M.; Raza, H.; Seo, S.Y.; Shabbir, G. Synthesis of 4-aryl-2, 6-dimethyl-3, 5-bis-N-(aryl)-carbamoyl-1, 4-dihydropyridines as novel skin protecting and anti-aging agents. *Bangladesh J. Pharmacol.* **2017**, *12*, 210–215. [[CrossRef](#)]
15. Kato, E.; Iwano, N.; Yamada, A.; Kawabata, J. Synthesis and  $\alpha$ -amylase inhibitory activity of glucose–deoxynojirimycin conjugates. *Tetrahedron* **2011**, *67*, 7692–7702. [[CrossRef](#)]
16. Patel, B.D.; Bhadada, S.V.; Ghate, M.D. synthesis and anti-diabetic activity of triazolotriazine derivatives as dipeptidyl peptidase-4 (DPP-4) inhibitors. *Bioorg. Chem.* **2017**, *72*, 345–358. [[CrossRef](#)]
17. Shahidpour, S.; Panahi, F.; Yousefi, R.; Nourisefat, M.; Nabipoor, M.; Ali Khalafi-Nezhad, A. Design and synthesis of new antidiabetic  $\alpha$ -glucosidase and  $\alpha$ -amylase inhibitors based on pyrimidine-fused heterocycles. *Med. Chem. Res.* **2015**, *24*, 3086–3096. [[CrossRef](#)]
18. Aslam, M.A.S.; Mahmood, S.U.; Shahid, M.; Saeed, A.; Iqbal, J. Synthesis, biological assay in vitro and molecular docking studies of new Schiff base derivatives as potential urease inhibitors. *Eur. J. Med. Chem.* **2011**, *46*, 5473–5479. [[CrossRef](#)]
19. Vigato, P.A.; Tamburini, S. The challenge of cyclic and acyclic Schiff bases and related derivatives. *Coord. Chem. Rev.* **2004**, *248*, 1717–2128. [[CrossRef](#)]
20. Karthikeyan, M.S.; Prasad, D.J.; Poojary, B.; Bhat, K.S.; Holla, B.S.; Kumari, N.S. Synthesis and biological activity of Schiff and Mannich bases bearing 2, 4-dichloro-5-fluorophenyl moiety. *Bioorg. Med. Chem.* **2006**, *14*, 7482–7489. [[CrossRef](#)]
21. Ren, S.; Wang, R.; Komatsu, K.; Bonaz-Krause, P.; Zyrianov, Y.; McKenna, C.E.; Csipke, C.; Tokes, Z.A.; Lien, E.J. Synthesis, biological evaluation, and quantitative structure– activity relationship analysis of new Schiff bases of hydroxysemicarbazide as potential antitumor agents. *J. Med. Chem.* **2002**, *45*, 410–419. [[CrossRef](#)] [[PubMed](#)]
22. Da Silva, C.M.; Da Silva, D.L.; Modolo, L.V.; Alves, R.B.; De Resende, M.A.; Martins, C.V.; De Fátima, Â. Schiff bases: A short review of their antimicrobial activities. *J. Adv. Res.* **2011**, *2*, 1–8. [[CrossRef](#)]
23. Vicini, P.; Geronikaki, A.; Incerti, M.; Busonera, B.; Poni, G.; Cabras, C.A.; La Colla, P. Synthesis and biological evaluation of benzo [d] isothiazole, benzothiazole and thiazole Schiff bases. *Bioorg. Med. Chem.* **2003**, *11*, 4785–4789. [[CrossRef](#)]
24. Borisova, N.E.; Reshetova, M.D.; Ustynyuk, Y.A. Metal-free methods in the synthesis of macrocyclic Schiff bases. *Chem. Rev.* **2007**, *107*, 46–79. [[CrossRef](#)] [[PubMed](#)]
25. Shi, L.; Ge, H.M.; Tan, S.H.; Li, H.Q.; Song, Y.C.; Zhu, H.L.; Tan, R.X. Synthesis and antimicrobial activities of Schiff bases derived from 5-chloro-salicylaldehyde. *Eur. J. Med. Chem.* **2007**, *42*, 558–564. [[CrossRef](#)]
26. Dinçalp, H.; Toker, F.; Durucasu, I.; Avcıbaşı, N.; İcli, S. New thiophene-based azo ligands containing azo methine group in the main chain for the determination of copper (II) ions. *Dyes Pigments* **2007**, *75*, 11–24. [[CrossRef](#)]
27. Kurtoglu, G.; Avar, B.; Zengin, H.; Kose, M.; Sayin, K.; Kurtoglu, M. A novel azo-azomethine based fluorescent dye and its Co (II) and Cu (II) metal chelates. *J. Mol. Liq.* **2014**, *200*, 105–114. [[CrossRef](#)]
28. Nejati, K.; Rezvani, Z.; Seyedahmadian, M. The synthesis, characterization, thermal and optical properties of copper, nickel, and vanadyl complexes derived from azo dyes. *Dyes Pigments* **2009**, *83*, 304–311. [[CrossRef](#)]
29. Refat, M.S.; El-Deen, I.M.; Anwer, Z.M.; El-Ghol, S. Spectroscopic studies and biological evaluation of some transition metal complexes of Schiff-base ligands derived from 5-arylaazo-salicylaldehyde and thiosemicarbazide. *J. Coord. Chem.* **2009**, *62*, 1709–1718. [[CrossRef](#)]
30. Hallas, G.; Towns, A.D. Synthesis of some nitro-substituted thiophene-based azo disperse dyes. *Dyes Pigments* **1997**, *33*, 319–336. [[CrossRef](#)]
31. Hallas, G.; Choi, J.H. Synthesis and spectral properties of azo dyes derived from 2-aminothiophenes and 2-aminothiazoles. *Dyes Pigments* **1999**, *42*, 249–265. [[CrossRef](#)]

32. Singh, H.; Sindhu, J.; Khurana, J.M.; Sharma, C.; Aneja, K.R. Syntheses, biological evaluation and photophysical studies of novel 1, 2, 3-triazole linked azo dyes. *RSC Adv.* **2014**, *4*, 5915–5926. [[CrossRef](#)]
33. Garjani, A.; Davaran, S.; Rashidi, M.; Malek, N. Protective effects of some azo derivatives of 5-aminosalicylic acid and their pegylated prodrugs on acetic acid-induced rat colitis. *Daru J. Pharm. Sci.* **2004**, *12*, 24–30.
34. Ono, M.; Wada, Y.; Wu, Y.; Nemori, R.; Jinbo, Y.; Wang, H.; Lo, K.M.; Yamaguchi, N.; Brunkhorst, B.; Otomo, H.; et al. FP-21399 blocks HIV envelope protein-mediated membrane fusion and concentrates in lymph nodes. *Nat. Biotechnol.* **1997**, *15*, 343. [[CrossRef](#)] [[PubMed](#)]
35. Larik, F.A.; Saeed, A.; Channar, P.A.; Ismail, H.; Dilshad, E.; Mirza, B. New 1-octanoyl-3-aryl thiourea derivatives: Solvent-free synthesis, characterization and multi-target biological activities. *Bangladesh J. Pharmacol.* **2016**, *11*, 894–902. [[CrossRef](#)]
36. Nepali, K.; Lee, H.-Y.; Liou, J.-J. Nitro-Group-Containing Drugs. *J. Med. Chem.* **2019**, *62*, 2851–2893. [[CrossRef](#)] [[PubMed](#)]
37. Ertl, P.; Rohde, B.; Selzer, P. Fast calculation of molecular polar surface area as a sum of fragment-based contributions and its application to the prediction of drug transport properties. *J. Med. Chem.* **2000**, *43*, 3714–3717. [[CrossRef](#)]
38. Ghose, A.K.; Herbertz, T.; Hudkins, R.L.; Dorsey, B.D.; Mallamo, J.P. Knowledge-based, central nervous system (CNS) lead selection and lead optimization for CNS drug discovery. *ACS Chem. Neurosci.* **2012**, *3*, 50–68. [[CrossRef](#)] [[PubMed](#)]
39. Bakht, M.A.; Yar, M.S.; Abdel-Hamid, S.G.; Al-Qasoumi, S.I.; Samad, A. Molecular properties prediction, synthesis and antimicrobial activity of some newer oxadiazole derivatives. *Eur. J. Med. Chem.* **2010**, *45*, 5862–5869. [[CrossRef](#)]
40. Tian, S.; Wang, J.; Li, Y.; Li, D.; Xu, L.; Hou, T. The application of in silico drug-likeness predictions in pharmaceutical research. *Adv. Drug Deliv. Rev.* **2015**, *86*, 2–10. [[CrossRef](#)]
41. Prerana, B.; Jadhav, A.; Yadav, R.; Megha, G.G. Concept of drug likeness in pharmaceutical research. *Int. J. Pharm. Bio Sci.* **2015**, *6*, 142–154.
42. Ertl, P.; Schuffenhauer, A. Estimation of synthetic accessibility score of drug-like molecules based on molecular complexity and fragment contributions. *J. Cheminform.* **2009**, *1*, 8. [[CrossRef](#)] [[PubMed](#)]
43. Cheng, A.C. Predicting selectivity and druggability in drug discovery. *Annu. Rep. Comput. Chem.* **2008**, *4*, 23–37.
44. Litterman, N.K.; Lipinski, C.A.; Bunin, B.A.; Ekins, S. Computational prediction and validation of an expert's evaluation of chemical probes. *J. Chem. Inf. Model.* **2014**, *54*, 2996–3004. [[CrossRef](#)] [[PubMed](#)]
45. Hassan, M.; Abbas, Q.; Ashraf, Z.; Moustafa, A.A.; Seo, S.Y. Pharmacoinformatics exploration of polyphenol oxidases leading to novel inhibitors by virtual screening and molecular dynamic simulation study. *Comput. Biol. Chem.* **2017**, *68*, 131–142. [[CrossRef](#)] [[PubMed](#)]
46. Ghosh, S.; Rangan, L. Molecular docking and inhibition studies of  $\alpha$ -amylase activity by labdane diterpenes from *Alpinia nigra* seeds. *Med. Chem. Res.* **2014**, *23*, 4836–4852. [[CrossRef](#)]
47. Abbas, Q.; Hassan, M.; Raza, H.; Kim, S.J.; Chung, K.W.; Kim, G.H.; Seo, S.Y. In vitro, in vivo and in silico anti-hyperglycemic inhibition by sinigrin. *Asian Pac. J. Trop. Med.* **2017**, *10*, 372–379. [[CrossRef](#)]

**Sample Availability:** Samples of the compounds are available from the authors.



© 2019 by the authors. Licensee MDPI, Basel, Switzerland. This article is an open access article distributed under the terms and conditions of the Creative Commons Attribution (CC BY) license (<http://creativecommons.org/licenses/by/4.0/>).